

# Geophysical Research Letters

## RESEARCH LETTER

10.1029/2020GL088440

### Key Points:

- In a novel approach, radars are automatically guided by external observations from satellite imagery and surface cameras
- First ever automated observations of rapidly evolving shallow cumulus, waterspouts, and lightning by a phased-array radar and a cloud radar
- Using external observation to guide radars constitutes a paradigm shift on how to sample the atmosphere

### Correspondence to:

P. Kollias,  
pavlos.kollias@stonybrook.edu

### Citation:

Kollias, P., Luke, E., Oue, M., & Lamer, K. (2020). Agile adaptive radar sampling of fast-evolving atmospheric phenomena guided by satellite imagery and surface cameras. *Geophysical Research Letters*, 45, e2020GL088440. <https://doi.org/10.1029/2020GL088440>

Received 15 APR 2020

Accepted 9 JUN 2020

Accepted article online 20 JUN 2020

## Agile Adaptive Radar Sampling of Fast-Evolving Atmospheric Phenomena Guided by Satellite Imagery and Surface Cameras

Pavlos Kollias<sup>1,2</sup> , Edward Luke<sup>2</sup>, Mariko Oue<sup>1</sup> , and Katia Lamer<sup>2</sup> 

<sup>1</sup>Division of Atmospheric Sciences, Stony Brook University, Stony Brook, NY, USA, <sup>2</sup>Environmental and Climate Sciences Department, Brookhaven National Laboratory, Upton, NY, USA

**Abstract** The collection of high temporal resolution radar observations without compromising data quality requires adaptability and agility. So far, radar beam steering has been mostly guided by (i) expert judgment or (ii) stand-alone automated identification and tracking algorithms operating on measurements collected by radar. The current study proposes a new paradigm, where external observations are used to optimize a radar's sampling strategy. Here the sampling strategy of a phased-array radar and a polarimetric scanning cloud radar, two different yet uniquely complementary systems, is guided by an algorithm that uses observations from a geostationary satellite, a surface camera and the radars themselves to identify and track atmospheric phenomena. The tailored pointing and increase in sensitivity realized through this framework enables the steered radars to sample a diverse set of atmospheric phenomena such as shallow cumuli, lightning-induced ice crystal orientation and a series of waterspouts.

### 1. Introduction

Since the early 1960s, radars have been the primary sensor for probing clouds and precipitation, serving a wide spectrum of applications ranging from climate studies to severe weather monitoring (Kollias et al., 2019). For data record continuity reasons among others, the majority of scanning radars have been operated with predetermined scan strategies not always optimum for the specific weather conditions at hand (McLaughlin et al., 2009; Miller et al., 1998).

Besides the handful of weather-chasing mobile scanning radars guided by expert field researchers (e.g., Bluestein et al., 2010; Pazmany et al., 2013; Wurman et al., 1997), only a few scanning radars systematically adapt their sampling strategy based on the actual atmospheric state. An example of this is the U.S. National Weather Service Weather Surveillance Radar-1988 Doppler (NEXRAD) network, which switches between clear-air and precipitation mode based on the weather (Chrisman, 2009).

One common characteristic of most current adaptive scan strategies (including the aforementioned) is that they rely on measurements collected by the radar itself while in surveillance mode to sense the atmospheric state and identify targets of interest. We will call this approach “stand alone,” highlighting the fact that it only relies on the use of the radar both to provide context and to collect targeted observations. We would argue that the “stand-alone” approach has three main drawbacks: It may not allow for (i) the detection of weakly reflective features because the scan rate required for performing surveillance *limits sensitivity* (this is important for targets like shallow cumuli), (ii) the monitoring of *fast-evolving* processes or *short-lived* systems because surveillance diverts resources away from sampling features of interest (this is important for mechanically scanning radars), and (iii) the targeting of cloud sectors experiencing unique *phenomenon not detectable by radar signals* (e.g., lightning).

Networks of radars have been employed to address some of the aforementioned challenges. An example of this is the Collaborative Adaptive Sensing of the Atmosphere (CASA) network (McLaughlin et al., 2009), a network of small, low-cost, short-range radars controlled by a software architecture, which automatically balances user preferences for information, data quality, system resources, and the evolving weather (Philips et al., 2008). Another example is the large mechanically scanning Chilbolton radar, which is automatically steered towards storms based on their size, rainfall rate, and distance from the radar using observations from the UK radar network (Stein et al., 2015). Although useful, the guidance provided by

©2020. The Authors.

This is an open access article under the terms of the Creative Commons Attribution-NonCommercial License, which permits use, distribution and reproduction in any medium, provided the original work is properly cited and is not used for commercial purposes.

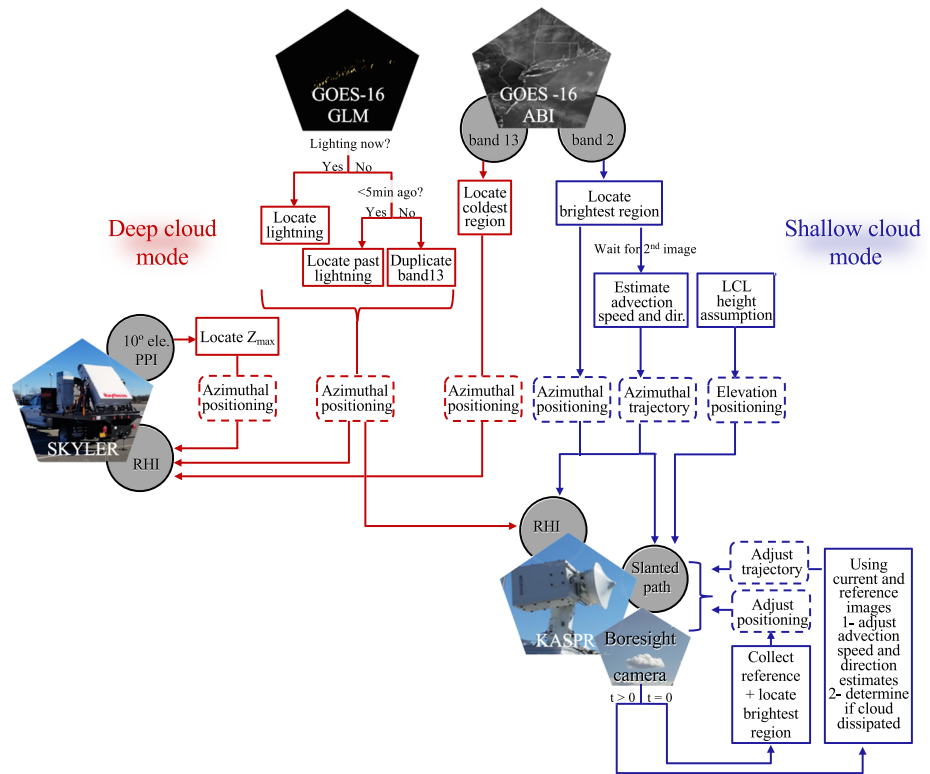


**Figure 1.** The MAAS framework is used to guide the scan strategy of the KASPR and the SKYLER radars using inputs from multiple sensors.

networks of radar is bound to the type of atmospheric features that generate radar signatures leaving gaps in our ability to target cloud sectors impacted by unique phenomenon such as lightning.

Here we propose a new radar sampling paradigm that relies on observations from external (radar and non-radar) sources - each uniquely sensitive to different parts of the atmospheric system - to steer radars. In this framework, which we call the Multisensor Agile Adaptive Sampling (MAAS), greater awareness of the atmospheric state is achieved, and rapid sequences of high-quality targeted radar scan can be collected all that without the need for a radar network but instead using a diversity of sensors.

This manuscript describes an implementation of this versatile framework as it is used to steer two fundamentally different yet uniquely complementary radars currently operating from the Stony Brook Radar Observatory (SBRO). Guidance by MAAS allowed radars to observe a shallow cloud over its life cycle and elusive short-term phenomena in deeper clouds including waterspouts and lightning-induced ice crystal orientation.

## 2. Implementation of the MAAS Framework

In this section, we describe an implementation of the MAAS framework used to automatically steer two collocated radars (section 2.1) when operating in either shallow (section 2.2) or deep (section 2.3) cloud mode. At the moment, user input is required to switch between modes.

### 2.1. Description of the Radars

KASPR is a mechanically scanning  $0.3^\circ$  beamwidth Ka-band polarimetric radar, which is an upgraded version of the Scanning Atmospheric radiation measurement Cloud Radars (SACR) described in Kollias, Bharadwaj, et al. (2014) and Kollias, Jo, et al. (2014) (Figure 1). KASPR collects standard radar moments: radar reflectivity ( $Z_{HH}$ ), mean Doppler velocity, and spectral width, as well polarimetric radar observables including: differential reflectivity ( $Z_{DR}$ ), differential phase ( $\phi_{DP}$ ), copolar correlation coefficient ( $\rho_{hv}$ ), linear depolarization ratio (LDR), cross-polar correlation coefficient ( $\rho_{hx}$ ), and specific differential phase ( $K_{DP}$ )

(Hubbert & Bringi, 1995). In the current study, KASPR was set to operate with pulse compression, a range gate spacing of 25 m, a maximum range of 30 km and to scan at a rate of  $6^\circ \text{ s}^{-1}$  yielding a sensitivity of  $-40 \text{ dBZ}$  at 1 km.

SKYLER is a dual-polarization, X-band, low-power, phased-array radar (Figure 1; Pavlos Kollias et al., 2018) with an antenna beam width of  $1.98^\circ$  in azimuth and  $2.1^\circ$  in elevation at boresight. The radar transmits H- and V-polarization pulses (alternate) and provides estimates of standard radar moments as well as of  $Z_{DR}$ ,  $\varphi_{DP}$ , and  $\rho_{hv}$ . Relative to its baseline position, SKYLER is capable of electronically scanning a sector of  $\pm 45^\circ$  in azimuth and electronically scanning a sector of  $0^\circ$ – $30^\circ$  in elevation. SKYLER's baseline position is mechanically controlled though not automatically at the moment; for the current study, SKYLER was positioned facing south at  $15^\circ$  elevation. SKYLER was set to operate with a range gate spacing of 100 m and a maximum range of 40 km and to scan at a rate of  $30^\circ \text{ s}^{-1}$  yielding a sensitivity better than 0 dBZ at 1 km.

## 2.2. Shallow Cloud Systems—Steering of a Mechanically Scanning Millimeter-wavelength Radar

Millimeter-wavelength radars, such as KASPR, with their generally excellent sensitivity tend to be preferred for the study of clouds and light precipitation (Kollias et al., 2016, 2007). That being said, their narrow antenna beam width requires operation at a slower scan rate in order to collect a sufficient number of samples to achieve detection of low signal-to-noise ratio echoes (Doviak & Zrnic, 1993). Under these conditions, approximately 10 min would be required to cover the hemispherical sky (i.e., a  $360^\circ$  azimuth sector at 10 different elevations at  $6^\circ \text{ s}^{-1}$ ), thus rendering impossible the complete sampling, let alone tracking, of fast evolving clouds such as shallow cumuli. Because of this limitation, among other things, millimeter-wavelength radars have typically been operated following a set of predetermined scan strategies, presumably suitable for the characterization of clouds (if so encountered) (e.g., Kollias, Bharadwaj, et al., 2014). Only on few occasions have these systems been fortuitous enough to collect snapshots of fast evolving atmospheric systems, notably by using range-height indicator (RHI) type scan strategies (Borque et al., 2014; Lamer et al., 2014).

During shallow cloud conditions, the MAAS framework (Figure 1) addresses the aforementioned challenges using surveillance provided by the Advanced Baseline Imager (ABI) onboard the GOES-16 satellite to guide KASPR.

Each sampling cycle starts with the acquisition of a snapshot from the finest spatial resolution ( $0.5$ – $1 \text{ km}^2$ ) visible red band (band 2) of the GOES-16 ABI, which is used to locate the brightest region within a 50-km radius around the observatory; the latitude and longitude of this feature are converted to azimuthal coordinates, which are sent to KASPR for initial positioning.

The advection speed and direction of the feature are then estimated by maximizing correlation with the next consecutive GOES-16 ABI snapshot within a 10-km radius around the feature (guaranteed available within 5 min but often captured as fast as every 1 min) and converted to an azimuthal trajectory for subsequent KASPR positioning. It is implied here that the accuracy of the advection estimates decreases for cloud fields shorter lived than the GOES-16 data cycle.

The initial azimuthal positioning and trajectory (for subsequent repositioning) are used to guide either of two scan types—an RHI sequence (section 2.1.1) or a slanted path (section 2.1.2)—each providing unique insight into short-lived shallow clouds. Note that because MAAS does not require the steered system to conduct its own surveillance to provide atmospheric context, it allows for a reduced scan rate (and increased scan time), thus generating a gain in sensitivity compared to “stand-alone” operation.

### 2.2.1. Slicing Through a Shallow Cloud System

When elected by the user, MAAS guides KASPR as it performs a sequence of RHI scans aiming to track a cloud entity. This sequence is guided by advection speed and direction estimates calculated using the two GOES-16 ABI snapshots collected at the beginning of the sampling cycle. To target for example shallow clouds forming and advecting from a distance  $\sim 15$ – $30 \text{ km}$  away from the radar, the RHI scans are set to cover an elevation sector between  $1^\circ$  to  $9^\circ$  at a  $0.3^\circ$  spacing (i.e., no gaps in elevation). The limited extent of the elevation sector allows for rapid updates, enabling the characterization of cumulus life cycle, an example of which is given in section 3.1. The RHI scan sequence is set to continue (without follow on input by GOES-16 ABI) until interrupted by the user. Follow on acquisition of updated GOES-16 ABI snapshots marks the beginning of a new sampling cycle.

### 2.2.2. Staring at a Shallow Cloud System

When elected by the user, MAAS guides KASPR as it performs a slanted path scan aiming to track a cloud entity. Slanted path scans additionally require information about the elevation of clouds above the horizon. An assumption about the lifting condensation level height is initially used to steer KASPR in the elevation direction. This position is refined using observations collected by a boresight camera installed on KASPR's pedestal, which records subsecond red-green-blue imagery collocated with the radar beam. A first snapshot (reference snapshot) from the boresight camera is used to slightly adjust the KASPR's pointing (both in azimuth and elevation) such that the brightest region within the boresight camera frame is centered. Subsequent snapshots from the boresight camera (every 5 s) are used to estimate/adjust advection speed in the elevation direction and adjust the azimuthal advection position and speed estimates initially obtained using GOES-16 visible imagery. Both are accomplished by maximizing the correlation between the current boresight camera snapshots and the reference boresight camera snapshot. Poor correlation between the snapshots is used as an indication that the feature has dissipated or morphed beyond recognition and triggers the end of the tracking sequence and of the sampling cycle. Follow on acquisition of updated GOES-16 ABI snapshots marks the beginning of a new sampling cycle.

### 2.3. Deep Cloud Systems—Steering of a Centimeter-Wavelength Phased-Array Radar and a Mechanically Scanning =Millimeter-Wavelength Radar

Although millimeter-wavelength radars may also provide insight into the properties of precipitation, they generally suffer from nonnegligible attenuation; for this reason, centimeter-wavelength radars tend to be preferred for the study of precipitation and weather monitoring (Kollias et al., 2019).

In the past few years, the adaptation of phased array technology to atmospheric applications has enabled near instantaneous positioning of the radar beam and nearly simultaneous independent monitoring of multiple spatially separated atmospheric features (Council, 2008). At the moment, only a handful of phased-array systems for atmospheric applications are operational, those include the Stony Brook Radar Observatory's SKYLER system (courtesy of Raytheon Company; Kollias et al., 2018) and the National Weather Radar Testbed (Torres et al., 2016).

Despite its many advantages, the current generation of phased-array radars can still benefit from being operated in a multisensor framework; especially when it comes to monitoring atmospheric vortices (i.e., tornadoes and waterspouts) that tend to form near the highest point of storms or when it comes acquiring high quality polarimetric data (Zhang et al., 2019).

During deep cloud conditions, MAAS automatically steers SKYLER and KASPR in the azimuthal direction for them to performed targeted RHI scans. As part of each sampling cycle, SKYLER is set to perform one “stand-alone” surveillance scan and three simultaneous RHI scans while KASPR is set to perform a single high-quality polarimetric RHI scan covering a sector, for example between 2° and 90°, along the path of one of SKYLER's RHI. MAAS relies on information from:

- i The “stand-alone” surveillance simultaneously performed by SKYLER, taking the form of a Plan Position Indicator (PPI) scan performed at 10° elevation covering SKYLER's full azimuthal range ( $\pm 45^\circ$  azimuth sector relative to the position of its manually steerable rotation table). SKYLER's first simultaneous RHI is aimed toward the azimuth of the highest reflectivity region in the surveillance scan between 0 and 30 km range.
- ii Surveillance observations from band 13 of the GOES-16 ABI (i.e., top-of-atmosphere outgoing longwave radiance, 1–2 km<sup>2</sup> resolution); SKYLER's second simultaneous RHI is aimed toward the azimuth of the coldest cloud top within a 50-km radius around the observatory.
- iii Surveillance provided by the GOES-16's Geostationary Lightning Mapper (GLM) (9.5-km pixel field of view) that can detect momentary changes in an optical scene for lightning detection (e.g., Goodman et al., 2013). Both SKYLER's third simultaneous RHI and KASPR's RHI are aimed towards the azimuth of the most recent lightning (within 1 min) or highest strike density (within 5 min), in that order of precedence. After 5 min of lightning inactivity, SKYLER and KASPR fall back to duplicate the RHI guided by the coldest cloud top (providing doubled temporal resolution for SKYLER).

Note that storm motion is currently not estimated in deep mode such that each identified feature of interest is not resampled as part of a single sampling cycle. That being said, since features of interest are often present

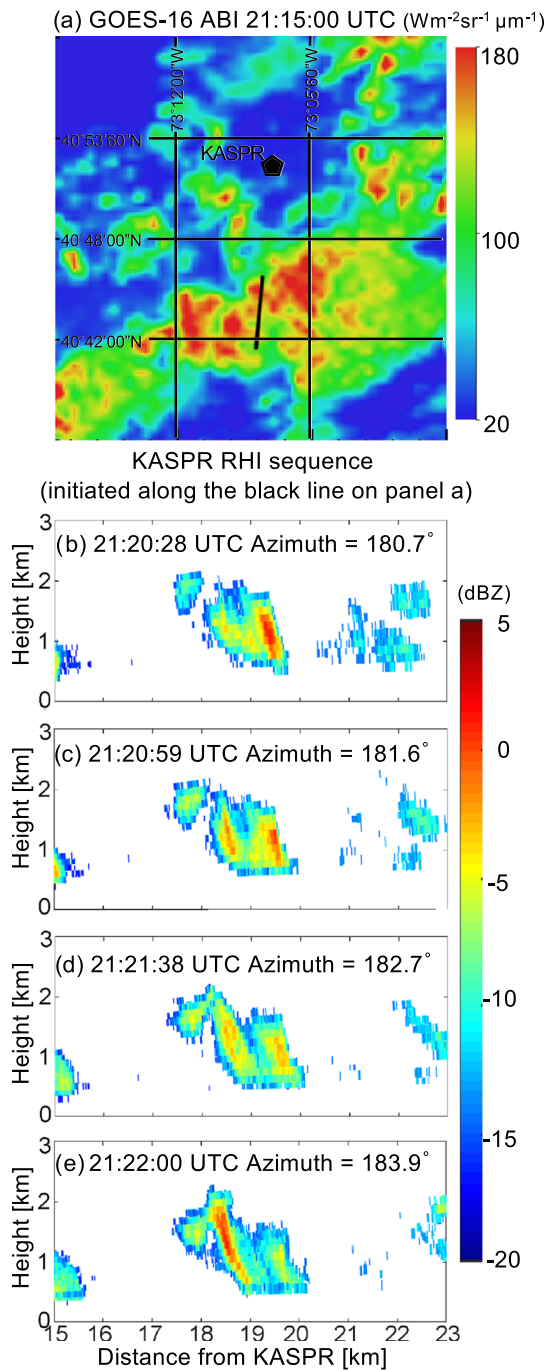


**Figure 2.** (a) Radiance recorded by GOES-16 ABI, (b-e) radar reflectivity recorded by the KASPR during an RHI sequence guided by the MAAS framework; the RHI scan sequence was initiated along the line depicted in panel (a) and the azimuthal position updated following MAAS guidance.

in subsequent surveillance scans (provided by SKYLER, the GOES-16 ABI and the GOES-16 GLM), they are often resampled several times over their life cycle over multiple sampling cycles. This mode enabled the observations of several waterspouts and of lighting-induced ice crystal orientation events, examples of which are given in sections 3.2 and 3.3, respectively.

### 3. Radar Observations of Fast Physics Enabled by MAAS

The MAAS framework enabled the agile deployment of KASPR and/or SKYLER for the monitoring of generally elusive short-lived atmospheric phenomena including (i) a shallow cumulus cloud along its lifecycle (section 3.1), waterspouts (section 3.2), and ice crystal orientation in a lightning producing storm (section 3.3).

#### 3.1. Shallow Cumulus Cloud Life Cycle

On 25 August 2019, a number of fair-weather shallow cumulus clouds were observed to form in the vicinity of the observatory. At 21:15:00 UTC, without any intervention from the KASPR radar, MAAS selected a bright target (i.e., a cloud) in the GOES-16 visible imagery (along the line Figure 2a). Following the collection of a second GOES-16 visible image (not shown), the advection speed and direction of this cloud was determined. This allowed MAAS to guide KASPR through a series of RHI scans at azimuthal locations adjusted to follow the estimated cloud trajectory. Because MAAS does not utilize any of KASPRs resources for surveillance, it allows for the uninterrupted collection of several vertical cross sections (i.e., RHIs) within the same evolving cloud. During this event, which began at 21:18:51 UTC and ended at 21:27:27 UTC, MAAS enabled KASPR to collect a total of 80 RHI scans each within 3–11 s apart proving a uniquely high-resolution uninterrupted view of the rapidly evolving shallow cumulus.

Figures 2b–2e show a subset of the RHI scans collected by KASPR during the event (not consecutive; only ranges between 15 and 23 km away from the radar location are shown corresponding to the location of the black line on Figure 2a). The radar reflectivity field can be used to visualize the roughly 2-km deep cumulus cloud(s) that formed just between 15 and 23 km away from the radar's location. Note the cellular structure of the cloud(s) with two distinct reflectivity maxima (one between 19.5 and 20 km and one between 18 and 19 km). Over time, the initially stronger cell is observed to weaken and the cloud top above it collapsing, while the other cell is observed to intensify and the cloud top above it rising. We estimate, based on the time from when the weaker cell was first observed to when it was last detected, that the cell's life cycle was roughly 9-min long.

Hopefully, MAAS will facilitate frequent observations of the internal structure of evolving shallow cumuli within their mesoscale context (as captured by the GOES-16 satellite; Figure 2a) and contribute to fill in some outstanding gaps in our understanding of shallow cloud lifecycle.

#### 3.2. Waterspouts

On 2 September 2019, the public reported several waterspouts on the south shore of Long Island. A rotation signature visible in the surveillance PPI scan collected by the National Weather Services' NEXRAD radar on Long Island (KOKX) suggests that a waterspout did form near Fire Island at 19:52 UTC (magenta dashed circle in Figure 3b). Minutes before, SKYLER also performed a PPI surveillance and detected not only one

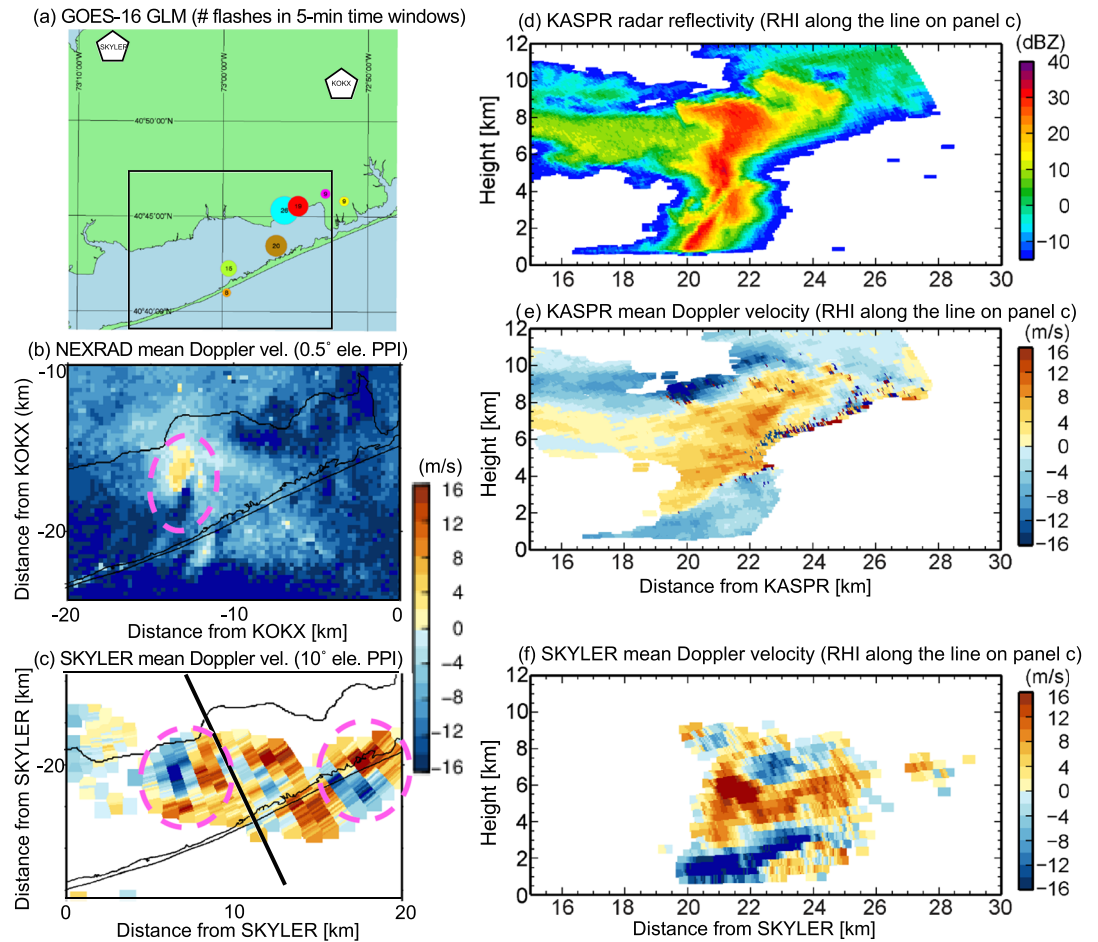


**Figure 3.** (a) Lighting strike density in 5-min time windows from 19:40 to 20:20 UTC (orange, green, brown, turquoise, red, and magenta, respectively) estimated from the GOES-16 GLM. For the region within the black rectangle in panel (a), (b) Doppler velocity recorded by the NEXRAD radar during a PPI scan at 19:52 UTC. (c) Doppler velocity recorded by the SKYLER during a PPI scan at 19:45 UTC. Magenta dashed circles indicate rotation signatures in panels (b) and (c). (d and e) radar reflectivity and Doppler velocity recorded by the KASPR during an RHI scan directed toward a lightning strike observed by the GOES-16 GLM along the trajectory marked by the black line on panel (c). (f) Doppler velocity simultaneously recorded by SKYLER for the same location. Note that negative Doppler velocity indicate motion toward the radars.

but two rotation signatures within the same sector (magenta dashed circles in Figure 3c). Based on the collection of subsequent SKYLER surveillance scans, we estimate that the waterspouts generally traveled east-northeastward and lasted between 10 and 15 min.

Besides reporting on the location of these waterspouts with clear horizontal rotation signatures and intensity reflectivity features, KASPR and SKYLER guided by MAAS sliced through a developing waterspout near Fire Island (Figures 3d–3f; range covering the black line on Figure 3c). Not evident in the “stand-alone” surveillance, the location of this developing waterspout coincided with that of multiple lighting flashes detected by the GOES-16 GLM, which information is used in the MAAS framework to guide the radars (lighting density in 5-min time windows from 19:40 to 20:20 UTC shown in Figure 3a). Although nearly simultaneous, the measurements collected by each of the radars differed, thus highlighting their unique complementarity and respective limitations (attenuation by rain for KASPR and lack of sensitivity to cloud for SKYLER). KASPR’s measurements reveal the impressive depth of the cloud supporting this rotating system the tops of which extended to 12 km (Figure 3d), while SKYLER’s measurements suggest that at its narrowest point this waterspout had to be at least 2-km wide (Figure 3f). SKYLER’s Doppler velocity measurements within the core of the waterspout reveal peak wind speeds of  $25 \text{ m s}^{-1}$  and suggest counterclockwise spiral rotation (as evidenced by the tilted Doppler velocity dipole in Figure 3f).

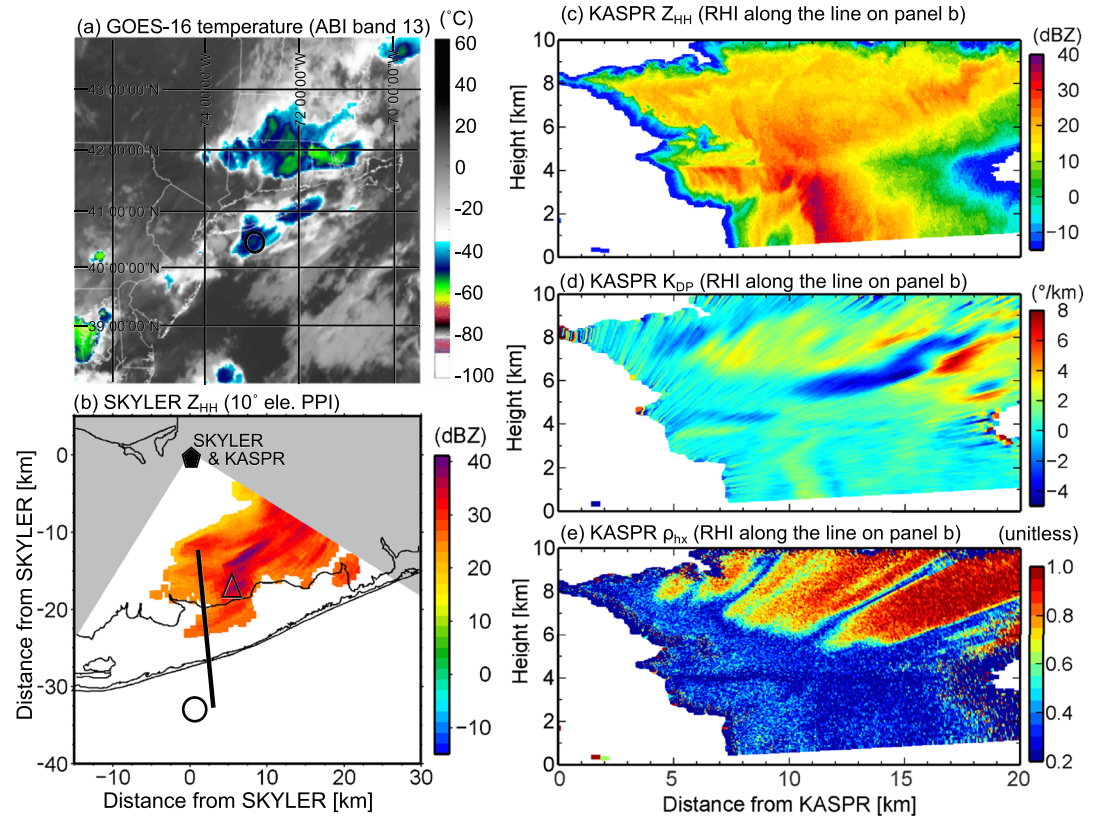


**Figure 4.** (a) Cloud top temperature recorded by the GOES-16 ABI at 23:27 UTC, (b) radar reflectivity recorded by SKYLER during a PPI scan at 23:30 UTC. (c) Radar reflectivity, (d) KDP, and (e)  $\rho_{hx}$  recorded by KASPR during an RHI scan directed toward a lightning strike observed by the GOES-16 GLM along the trajectory marked by the black line on panel (b). Under guidance from MAAS, RHIs were also collected by SKYLER in the direction of the coldest cloud top (circle in panel (a) and (b)) and the highest reflectivity echo in SKYLER's PPI surveillance (triangle in panel (b)).

Under the automatic guidance of the MAAS framework, KASPR was able to monitor the evolution of this waterspout from its generally poorly documented early stage to its mature stage, intersecting it every 40 s, while SKYLER RHI's toggled between several waterspouts.

### 3.3. Ice Crystal Orientation in a Lightning Producing Storm

On 21 August 2019, the GOES-16 GLM detected several lightning flashes on the South shore of Long Island (not shown). To gather unique insight on the internal structure of lightning producing convective cells, KASPR, which itself cannot detect lightning, was deployed by MAAS to slice through the convective cell located in the region of greatest lightning flash density reported by the GOES-16 GLM (Figures 4c–4e range covering the black line on Figure 4b).

KASPR recorded a bright band around 4 km suggesting that the storm contained both ice aloft and rain below (Figure 4c). Below the melting layer, KASPR recorded radar reflectivity as high as 40 dBZ within the convective core (note that radar reflectivity measurements beyond the core are attenuated). Above the melting layer, KASPR recorded negative specific differential phase ( $K_{DP}$ ,  $< -4^\circ \text{ km}^{-1}$ ; less affected by attenuation) and large cross-polar correlation coefficient ( $\rho_{hx}$ ,  $> 0.6$ ). Combined, these suggest the presence of prolate ice particles vertically oriented through lightning-induced electrification (Biggerstaff et al., 2017; Ryzhkov et al., 2002).

Under the automatic guidance of the MAAS framework, KASPR was able to monitor the evolution of this lightning producing convective cell, intersecting it every 40 s for 80 min. Hopefully, some of the radar signatures it detected can be associated to processes such as lightning cessation and help in the development of predictive schemes. Additional simultaneous RHIs were also collected by SKYLER (not shown) in the

direction of the coldest cloud top (i.e., circle in Figures 4a and 4b) and of the highest reflectivity echo in SKYLER's own PPI surveillance (triangle in Figure 4b).

#### 4. Summary and Future Plans

In remote sensing, it is not uncommon to rely on multiple sensors to observe different parts of the clear and cloudy atmosphere. Traditionally, their measurements are combined following data collection to improve the interpretation of processes using inversion techniques. Here multisensor measurements are used *in real time* to optimize the spatial–temporal sampling of atmospheric processes via agile adaptive sensing. The proposed MAAS framework overcomes challenges associated with relying on a single observing system (i.e., radar) both for locating, tracking and sampling features of interest.

An implementation of the general MAAS framework is used to steer two unique radars: KASPR a mechanically scanning Ka-band polarimetric radar and SKYLER a phased-array X-band polarimetric radar. In this implementation, depending on the atmospheric conditions (shallow or deep clouds), a combination of observations collected by the GOES-16 ABI, the GOES-16 GLM and/or a visible camera installed on KASPR's boresight is used to locate and estimate the advective trajectory of atmospheric features of interest for their tracking by the radars.

To our knowledge, this constitutes the first time that a high-quality, mechanically scanning polarimetric cloud radar has performed coordinated scans in conjunction with an electronically scanning radar. The mechanically scanning KASPR was dedicated to slow scan rate, high quality scans while the agile phased-array SKYLER instantaneously interrogated many different parts of a storm and provided high temporal resolution updates. This particular combination of radar resources steered by the MAAS framework has the potential to provide a leap forward in our ability to understand rapidly evolving microphysical and dynamical processes in cloud and precipitation systems.

KASPR and SKYLER guided by MAAS were shown capable of collecting unique information about the internal structure of (i) a multicell cumulus cloud along its 9-min life cycle at subminute temporal resolution, (ii) a forming waterspout, and (iii) a lightning producing convective system likely containing vertically oriented ice crystals as evidenced by high-quality polarimetric signatures.

In future expansions, MAAS could rely on observations from other operational sensors such as (i) the NEXRAD, which provides information about far range targets, (ii) networks of surface cameras, and (iii) lidars, which are sensitive to cloud base height and clear air dynamics. Since the MAAS framework includes the use of radar observations as input it can be completely “stand alone” if needed. This possibility is already implemented in the “deep cloud mode” and could easily be implemented in the “shallow cloud mode” by for example having KASPR perform one PPI scan at an arbitrary elevation and then having it scan through the highest reflectivity target identified in that surveillance scan. Beyond providing guidance for steering radars, the MAAS framework could also be used to manage sensor operations in power limited environments like buoys and CubeSat's (Peral et al., 2019).

#### Acknowledgments

Special thanks to Raytheon Company. The authors are supported by the Department of Energy Atmospheric System Research program. All the data used can be found in the Stony Brook University repository (<https://commons.library.stonybrook.edu/somasdata/>).

#### References

- Biggerstaff, M. I., Zounes, Z., Alford, A. A., Carrie, G. D., Pilkey, J. T., Uman, M. A., & Jordan, D. M. (2017). Flash propagation and inferred charge structure relative to radar-observed ice alignment signatures in a small Florida mesoscale convective system. *Geophysical Research Letters*, *44*, 8027–8036. <https://doi.org/10.1002/2017GL074610>
- Bluestein, H. B., French, M. M., PopStefanija, I., Bluth, R. T., & Knorr, J. B. (2010). A mobile, phased-array Doppler radar for the study of severe convective storms. *Bulletin of the American Meteorological Society*, *91*(5), 579–600. <https://doi.org/10.1175/2009bams2914.1>
- Borquez, P., Kollias, P., & Giangrande, S. (2014). First observations of tracking clouds using scanning ARM cloud radars. *Journal of Applied Meteorology and Climatology*, *53*(12), 2732–2746. <https://doi.org/10.1175/JAMC-D-13-0182.1>
- Chrisman, J. N. (2009). *Automated Volume Scan Evaluation and Termination (AVSET)*. Paper Presented at 34th Conference on Radar Meteorology.
- Council, N. R. (2008). *Evaluation of the multifunction phased array radar planning process*. Washington, DC: National Academies Press.
- Doviak, R., & Zrnic, D. (1993). Doppler radar and weather observations academic. San Diego, CA.
- Goodman, S. J., Blakeslee, R. J., Koshak, W. J., Mach, D., Bailey, J., Buechler, D., et al. (2013). The GOES-R geostationary lightning mapper (GLM). *Atmospheric Research*, *125*, 34–49.
- Hubbert, J., & Bringi, V. (1995). An iterative filtering technique for the analysis of copolar differential phase and dual-frequency radar measurements. *Journal of Atmospheric and Oceanic Technology*, *12*(3), 643–648. [https://doi.org/10.1175/1520-0426\(1995\)012%3C0643:AIFTF%3E2.0.CO;2](https://doi.org/10.1175/1520-0426(1995)012%3C0643:AIFTF%3E2.0.CO;2)
- Kollias, P., Bharadwaj, N., Clothiaux, E., Lamer, K., Oue, M., Hardin, J., et al. (2019). The ARM radar network: At the leading-edge of cloud and precipitation observations. *Bulletin of the American Meteorological Society*.

- Kollias, P., Bharadwaj, N., Widener, K., Jo, I., & Johnson, K. (2014). Scanning ARM cloud radars. Part I: Operational sampling strategies. *Journal of Atmospheric and Oceanic Technology*, *31*(3), 569–582.
- Kollias, P., Clothiaux, E. E., Ackerman, T. P., Albrecht, B. A., Widener, K. B., Moran, K. P., et al. (2016). Development and applications of ARM millimeter-wavelength cloud radars. *Meteorological Monographs*, *57*, 17.11–17.19.
- Kollias, P., Jo, I., Borque, P., Tatarevic, A., Lamer, K., Bharadwaj, N., et al. (2014). Scanning ARM cloud radars. Part II: Data quality control and processing. *Journal of Atmospheric and Oceanic Technology*, *31*(3), 583–598.
- Kollias, P., McLaughlin, D., Frasier, S., Oue, M., Luke, E., & Sneddon, A. (2018). *Advances and applications in low-power phased array X-band weather radars*. Paper presented at 2018 IEEE radar conference (RadarConf18), IEEE.
- Kollias, P., Miller, M. A., Luke, E. P., Johnson, K. L., Clothiaux, E. E., Moran, K. P., et al. (2007). The atmospheric radiation measurement program cloud profiling radars: Second-generation sampling strategies, processing, and cloud data products. *Journal of Atmospheric and Oceanic Technology*, *24*(7), 1199–1214. <https://doi.org/10.1175/JTECH2033.1>
- Lamer, K., Tatarevic, A., Jo, I., & Kollias, P. (2014). Evaluation of gridded scanning ARM cloud radar reflectivity observations and vertical doppler velocity retrievals. *Atmospheric Measurement Techniques*, *7*(4), 1089–1103. <https://doi.org/10.5194/amt-7-1089-2014>
- McLaughlin, D., Pepyne, D., Chandrasekar, V., Philips, B., Kurose, J., Zink, M., et al. (2009). Short-wavelength technology and the potential for distributed networks of small radar systems. *Bulletin of the American Meteorological Society*, *90*(12), 1797–1818. <https://doi.org/10.1175/2009BAMS2507.1>
- Miller, M. A., Verlinde, J., Gilbert, C. V., Lehenbauer, G. J., Tongue, J. S., & Clothiaux, E. E. (1998). Detection of nonprecipitating clouds with the WSR-88D: A theoretical and experimental survey of capabilities and limitations. *Weather and Forecasting*, *13*(4), 1046–1062. [https://doi.org/10.1175/1520-0434\(1998\)013%3C1046:DONCWT%3E2.0.CO;2](https://doi.org/10.1175/1520-0434(1998)013%3C1046:DONCWT%3E2.0.CO;2)
- Pazmany, A. L., Mead, J. B., Bluestein, H. B., Snyder, J. C., & Houser, J. B. (2013). A mobile rapid-scanning X-band polarimetric (RaXPol) Doppler radar system. *Journal of Atmospheric and Oceanic Technology*, *30*(7), 1398–1413. <https://doi.org/10.1175/JTECH-D-12-00166.1>
- Peral, E., Tanelli, S., Statham, S., Joshi, S., Imken, T., Price, D., et al. (2019). RainCube: The first ever radar measurements from a CubeSat in space. *Journal of Applied Remote Sensing*, *13*(3), 032504.
- Philips, B., Westbrook, D., Pepyne, D., Brotzge, J., Bass, E. J., & Rude, D. (2008). *User evaluations of adaptive scanning patterns in the CASA spring experiment 2007*. Paper presented at IGARSS 2008-2008 IEEE international geoscience and remote sensing symposium, IEEE.
- Ryzhkov, A. V., Zrnic, D. S., Hubbert, J. C., Bringi, V., Vivekanandan, J., & Brandes, E. A. (2002). Polarimetric radar observations and interpretation of co-cross-polar correlation coefficients. *Journal of Atmospheric and Oceanic Technology*, *19*(3), 340–354. <https://doi.org/10.1175/1520-0426-19.3.340>
- Stein, T. H., Hogan, R. J., Clark, P. A., Halliwell, C. E., Hanley, K. E., Lean, H. W., et al. (2015). The DYMECS project: A statistical approach for the evaluation of convective storms in high-resolution NWP models. *Bulletin of the American Meteorological Society*, *96*(6), 939–951. <https://doi.org/10.1175/BAMS-D-13-00279.1>
- Torres, S. M., Adams, R., Curtis, C. D., Forren, E., Forsyth, D. E., Ivić, I. R., et al. (2016). Adaptive-weather-surveillance and multifunction capabilities of the National Weather Radar Testbed phased array radar. *Proceedings of the IEEE*, *104*(3), 660–672. <https://doi.org/10.1109/JPROC.2015.2484288>
- Wurman, J., Straka, J., Rasmussen, E., Randall, M., & Zahrai, A. (1997). Design and deployment of a portable, pencil-beam, pulsed, 3-cm Doppler radar. *Journal of Atmospheric and Oceanic Technology*, *14*(6), 1502–1512. [https://doi.org/10.1175/1520-0426\(1997\)014%3C1502:DADOAP%3E2.0.CO;2](https://doi.org/10.1175/1520-0426(1997)014%3C1502:DADOAP%3E2.0.CO;2)
- Zhang, G., Mahale, V. N., Putnam, B. J., Qi, Y., Cao, Q., Byrd, A. D., et al. (2019). Current status and future challenges of weather radar polarimetry: Bridging the gap between radar meteorology/hydrology/engineering and numerical weather prediction. *Advances in Atmospheric Sciences*, *36*(6), 571–588. <https://doi.org/10.1007/s00376-019-8172-4>